

# Revisiting the Thickness of the Air–Water Interface from Two Extremes of Interface Hydrogen Bond Dynamics

Gang Huang and Jie Huang\*

Cite This: *J. Chem. Theory Comput.* 2024, 20, 9107–9115

Read Online

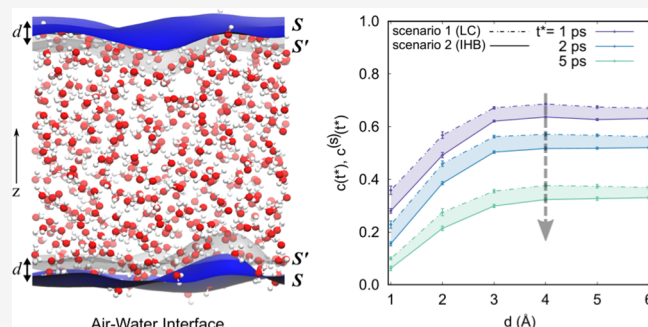
ACCESS |

Metrics &amp; More

Article Recommendations

Supporting Information

**ABSTRACT:** The air–water interface plays a crucial role in many aspects of science because of its unique properties, such as a two-dimensional hydrogen bond (HB) network and completely different HB dynamics compared to bulk water. However, accurately determining the boundary of interfacial and bulk water, that is, the thickness of the air–water interface, still challenges experimentalists. Various simulation-based methods have been developed to estimate the thickness, converging on a range of approximately 3–10 Å. In this study, we introduce a novel approach, grounded in density functional theory-based molecular dynamics and deep potential molecular dynamics simulations, to measure the air–water interface thickness, offering a different perspective based on prior research. To capture realistic HB dynamics in the air–water interface, two extreme scenarios of the interface HB dynamics are obtained: one underestimates the interface HB dynamics, while the other overestimates it. Surprisingly, our results suggest that the interface HB dynamics in both scenarios converges as the thickness of the air–water interface increases to 4 Å. This convergence point, indicative of the realistic interface thickness, is also validated by our calculation of anisotropic decay of OH stretch and the free OH dynamics at the air–water interface.



## 1. INTRODUCTION

The air–water interface has been the subject of extensive study due to its ubiquity in nature and its unusual macroscopic properties as a model system for aqueous hydrophobic interfaces.<sup>1–16</sup> It is widely accepted that water molecules behave in a completely different manner at the interface than in the bulk phase.<sup>17–19</sup>

Advances in the study of hydrogen bond (HB) dynamics at the air–water interface have been significant. Liu et al.<sup>20</sup> used molecular dynamics (MD) simulations to demonstrate faster HB breaking and forming at the interface than bulk water, attributed to quicker translational diffusion. From sum frequency generation (SFG) vibrational spectroscopy, Gan et al.<sup>21</sup> found that at the air–water interface, singly hydrogen (H)-bonded water molecules align almost parallel to the interface with limited orientational variation, while doubly H-bonded donor molecules orient their dipole vectors away from the liquid phase, highlighting diverse behaviors among interfacial water molecules. Almost concurrently, through time-resolved SFG vibrational spectroscopy, McGuire and Shen<sup>22</sup> observed ultrafast vibrational dynamics at the interface, noting that the relaxation behaviors of interfacially bonded OH stretch modes on subpicosecond time scales were akin to those in bulk water, encompassing spectral diffusion, vibrational relaxation, and thermalization. Pioneering work by Tahara's group,<sup>23,24</sup> which presented the first two-dimensional heterodyne-detected vibrational SFG (2D HD-VSFG) spectra of the

OH stretch region at the interface, highlighted diverse behaviors among interfacial HB OH groups. Subsequent studies, including those by Jeon et al.<sup>25</sup> and Ojha and Kühne,<sup>26</sup> have used MD and ab initio MD (AIMD) simulations to explore the structure and dynamics of interfacial water, uncovering weaker H-bonds and faster vibrational spectral dynamics of free OH groups compared to H-bonded OH groups at the interface. These collective insights enhance our understanding of the vibrational energy relaxation, HB dynamics, and interactions of water molecules at the air–water interface. Building upon this knowledge of interfacial behavior, significant efforts have also been directed toward quantifying the physical characteristics of the interface, including its thickness, which plays a crucial role in understanding its molecular interactions and behavior.

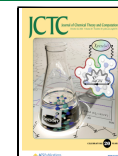
The air–water interface thickness has been measured via ellipsometry,<sup>27–29</sup> relative permittivity measurements,<sup>30</sup> X-ray reflectivity,<sup>31,32</sup> SFG spectroscopy,<sup>23,33–41</sup> classical MD simulations<sup>20,42–51</sup> and the AIMD simulations<sup>25,41,52–55</sup> to mention

Received: April 6, 2024

Revised: September 15, 2024

Accepted: September 24, 2024

Published: October 4, 2024



just a few. There is a consensus that the thickness of the air–water interface is about 3–10 (Å).<sup>42,43,45–47,52,54,56–59</sup> Nonetheless, accurately determining the thickness remains experimentally challenging. The MD and Monte Carlo (MC) simulations of the air–water interface yield molecular-level information not readily available in experiments. These simulations, which utilize various intermolecular potential functions, have played a crucial role in estimating the thickness.<sup>41,60–67</sup> Additionally, density functional theory-based MD (DFTMD) simulations<sup>52,68–73</sup> also offer a predictive platform for understanding density profiles and determining the thickness of the air–liquid interfaces.<sup>52,54,74,75</sup>

Nevertheless, DFTMD simulations are constrained by limitations in time and the number of molecules they can model. Traditional force field approaches, however, often lack the accuracy required to describe complex interface systems.<sup>76</sup> Recently, deep potential molecular dynamics (DeePMD) simulations based on machine learning potential (MLPs) have emerged as a promising alternative, offering a solution to the accuracy-versus-efficiency dilemma in molecular simulations.<sup>77</sup> One of the most accurate MLPs for water is MB-pol, which accurately reproduces many properties of water across the phase diagram.<sup>78–82</sup> Moreover, MB-pol has been used to obtain the VSFG and surface tension of air–water interface, demonstrating excellent agreement between theoretical predictions and experimental measurements.<sup>83</sup>

Inspired by the above experimental and simulation results, and with the motivation of capturing realistic HB dynamics at interfaces, we have designed an approach based on two extreme scenarios of interface HB dynamics by utilizing the trajectories of DFTMD and DeePMD simulations based on MB-pol. In the first scenario, for the set of molecules located in the interface layer at given sampling times, we use the Luzar-Chandler (LC) HB population operator<sup>84</sup> to obtain the HB dynamics of these interface molecules. In the second scenario, taking inspiration from Luzar and Chandler's HB population and the characteristic function introduced by Giberti and Hassanali,<sup>85</sup> we have developed an interface HB (IHB) population operator. This operator aims to provide a refined understanding of HB dynamics specifically at the interface.

The Luzar-Chandler HB population is utilized to describe whether a pair of labeled molecules form H-bonds. And the characteristic function developed by Giberti and Hassanali describes whether a specific molecule belongs to the interface region. Therefore, our newly defined interface HB population can describe whether a labeled pair of molecules is within the interface *and* connected by H-bonds at any given moment. This dual condition provides a more detailed understanding of interfacial HB dynamics.

Due to the thermal motion of water molecules, two scenarios may occur. In the first scenario, the water molecules under observation might transition into the bulk phase. In the second scenario, if a water molecule resides in the interface region *and* its H-bonded partner moves outside the interface area, then such a pair of molecules will no longer be of concern. Based on the study of interfacial water dynamics by Liu et al.,<sup>20</sup> Gan et al.,<sup>21</sup> Singh et al.,<sup>23</sup> and Jeon et al.,<sup>25</sup> as well as the investigation into the time-dependent spectral evolution of H-bonded and free water molecules by Ojha and Kühne,<sup>26</sup> our approach indicates that the HB dynamics derived from the first scenario will be slower the genuine interfacial HB dynamics. Conversely, the one obtained from the second scenario will exhibit faster dynamics than the genuine one.

Building upon the foundation laid by methods reliant on the density criterion,<sup>1,63–66,86–90</sup> our approach introduces an alternative way of determining interface thickness through the analysis of the convergence of interfacial HB dynamics properties. This approach effectively bypasses the necessity of accounting for liquid density. As such, it offers another perspective for measuring the thickness of the air–water interface. Furthermore, the principles underlying our approach hold potential for application to a broader range of systems, such as solution interfaces and ion shells, offering a flexible tool for interface studies.

## 2. METHODS

Due to molecular motions, the identity of molecules at the interface changes with time, and generally useful procedures for identifying interfaces must accommodate these motions. The air–water boundary is modeled with the Willard-Chandler instantaneous surface.<sup>48,75,91</sup> Figure 1 illustrates the obtained interfaces for one configuration of a slab of water.

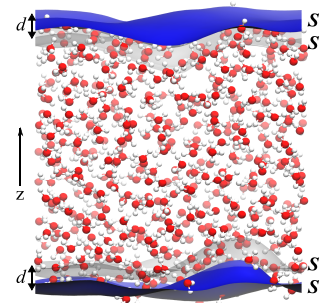


**Figure 1.** Slab of water containing 512 water molecules with the instantaneous surface  $S$  represented as a blue mesh on the upper and lower phase boundary. Gray surface, which represents an imaginary interface  $S'$ , is obtained by translating the surface to the inside of the system along the normal ( $z$ -axis) by distance  $d$ . This variable  $d$  is then utilized to measure the thickness of the air–water interface.

For the slab in the cuboid simulation box, an imaginary surface  $S'(t)$  is obtained by translating the surface  $S(t)$  along the system's normal (into bulk) to a distance  $d$ . The region between the two surfaces  $S(t)$  and  $S'(t)$  is defined as the air–water interface. Below we will combine two extreme scenarios to investigate the HB dynamics at the instantaneous air–water interface.

**2.1. Scenario 1: HB Dynamics Based on the Luzar-Chandler HB Population.** As the first scenario we use the Luzar-Chandler HB population and employ a technique that samples water molecules right at the instantaneous interface for certain sampling time points. In Scenario 1, we divide the simulation trajectory into multiple subtrajectories of length  $t_{\text{traj}}$ . Within these subtrajectories, the majority of water molecules exhibit thermal fluctuations near their equilibrium positions. Meanwhile, a select group of molecules initially at the interface may transition into the bulk phase at a later time. Due to the inclusion of H-bonds in the bulk phase, this scenario tends to underestimate the breaking rate of the H-bonds at the interface. In Section 3 of this paper, we will see this result, combined with the outcome from Scenario 2, can be used to estimate the thickness of the air–water interface. This method includes three steps as follows:

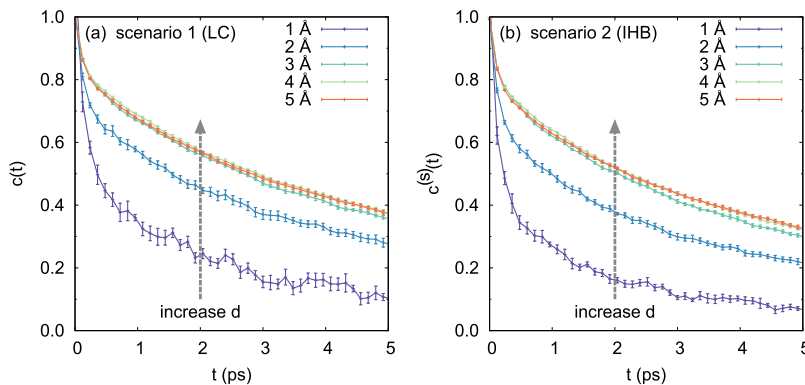


**Figure 2.** Autocorrelation functions  $c(t)$  and  $c^{(s)}(t)$  for interface H-bonds with different thickness  $d$  for (a) Scenario 1 (LC) and (b) Scenario 2 (IHB). Two notable features emerge: (i) As  $d$  increases, both  $c(t)$  and  $c^{(s)}(t)$  eventually approach a stable function. (ii) Decay rate of  $c^{(s)}(t)$  in Scenario 2 is greater than that of  $c(t)$  in Scenario 1. This behavior is visually represented by two dashed directed line segments, positioned identically to the graphs. Functions  $c(t)$  and  $c^{(s)}(t)$  on a log–log scale are also plotted in Supporting Information.

**a. Subtrajectories.** Subtrajectories with a specific length of time,  $t_{\text{traj}}$ , are selected. In this work,  $t_{\text{traj}}$  is set to be 40 (ps), which is long enough to observe HB dynamics but short enough that not all the molecules complete their transition across the interface.<sup>92</sup>

**b. Sampling.** For each time step, we identify a pair of the air–water interfaces of a specified thickness  $d$  as shown in Figure 1. At evenly spaced moments within  $t_{\text{traj}}$ , we select the water molecules within the interfaces. For the union of the interfacial water molecules picked at all these time moments, the Luzar-Chandler HB population-based correlation functions<sup>84</sup> across the subtrajectory are calculated.

**c. Statistics.** The average correlation functions across all subtrajectories are calculated.

In this scenario, the computational procedure for calculating HB dynamics follows the same methodology as that used in works based on the Luzar-Chandler's method (LC method).<sup>20,93,94</sup> For details on this method, please refer to the Supporting Information.

## 2.2. Scenario 2: HB Dynamics Based on Interface HB Population.

To capture the other extreme of interfacial HB dynamics, after determining the instantaneous interface, we introduce an interface HB population operator  $h^{(s)}[\mathbf{r}(t)]$  as follows: It has a value of 1 when a tagged molecular pair  $i, j$  are H-bonded and both molecules are at the interface with a thickness  $d$ , and 0 otherwise:

$$h^{(s)}[\mathbf{r}(t)] = \begin{cases} 1 & \mathbf{r}_i \in \mathcal{I}(d; t), \mathbf{r}_j \in \mathcal{I}(d; t), \\ & j \in \mathcal{B}_i(t); \\ 0 & \text{otherwise} \end{cases} \quad (1)$$

where  $\mathbf{r}(t)$  is the configuration of the system at time  $t$ ,  $\mathbf{r}_i$  is the position coordinate of the oxygen atom in the  $i$ th water molecule,  $\mathcal{B}_i(t)$  denotes the set of water molecules that are H-bonded with molecule  $i$  at time  $t$ , and  $\mathcal{I}(d; t)$  is the instantaneous interface layer with thickness  $d$  at time  $t$ . The definition of  $h^{(s)}$  combines the Luzar-Chandler's HB population<sup>84,95</sup>  $h$  and the characteristic function introduced by Giberti and Hassanali.<sup>85</sup> Then the correlation function  $c^{(s)}(t)$  that describes the fluctuation of H-bonds at the interface:

$$c^{(s)}(t) = \frac{\langle h^{(s)}(0)h^{(s)}(t) \rangle}{\langle h^{(s)} \rangle} \quad (2)$$

can be obtained. Similar to functions  $n(t)$  and  $k(t)$  in ref 84 (eqs 1 and 2 in Supporting Information), the corresponding correlation function

$$n^{(s)}(t) = \frac{\langle h^{(s)}(0)[1 - h^{(s)}(t)]h^{(d,s)} \rangle}{\langle h^{(s)} \rangle} \quad (3)$$

and interface reactive flux function

$$k^{(s)}(t) = -\frac{dc^{(s)}(t)}{dt} \quad (4)$$

are obtained. The  $h^{(d,s)}(t)$  is 1 when a tagged pair of water molecules  $i, j$  is at the interface and the interoxygen distance between the two molecules is less than the cutoff radius  $r_{\text{OO}}^c$  at time  $t$ , and 0 otherwise, i.e.,

$$h^{(d,s)}[\mathbf{r}(t)] = \begin{cases} 1 & \mathbf{r}_i \in \mathcal{I}(d; t), \mathbf{r}_j \in \mathcal{I}(d; t), \\ & |\mathbf{r}_i - \mathbf{r}_j| < r_{\text{OO}}^c; \\ 0 & \text{otherwise.} \end{cases} \quad (5)$$

Therefore,  $n^{(s)}(t)$  represents the probability at time  $t$  that a tagged pair of initially H-bonded water molecules at the interface are unbonded but remain at the interface and separated by less than  $r_{\text{OO}}^c$ ;  $k^{(s)}(t)$  measures the effective decay rate of H-bonds at the interface. The functions defined in eqs 2–4 are used to determine the reaction rate constants of breaking and reforming and the lifetimes of H-bonds at the interface by<sup>73,84</sup>

$$k^{(s)}(t) = kc^{(s)}(t) - k'n^{(s)}(t)$$

In this IHB scenario, choosing the water molecules and H-bonds at the interface is accurate. However, for some special H-bonds, if it connects such two water molecules, one is at the interface and the other is in the bulk phase, the HB breaking reaction rate of such H-bonds will be increased. Therefore, in contrast to the LC method used in Scenario 1, the IHB method used in this scenario overestimates the HB breaking rate constant.

The actual HB dynamics at the interface are expected to lie between the results obtained by the LC method and the IHB

method. Consequently, by integrating these two scenarios, we can achieve a more precise characterization of HB dynamics at the interface.

### 3. RESULTS AND DISCUSSIONS

In this section, we apply our two-extreme approach to two system properties: HB population autocorrelation functions and HB reaction rate constants. We then determine the thickness of the air–water interface based on each of these properties. The computational details for DFTMD and DeePMD simulations are available in the [Supporting Information](#). The results discussed in the following sections are derived from the trajectory data of the system containing 512 water molecules, modeled by MB-pol potential. Similar analyses for DFTMD simulations with 128 water molecules, and other system sizes in DeePMD simulations using MB-pol, are also provided in the [Supporting Information](#). The finite size effects of the main properties discussed in this article are also analyzed in [Supporting Information](#).

**3.1. HB Population Autocorrelation Functions.** Figure 2 illustrates the dynamic evolution of  $c(t)$  and  $c^{(s)}(t)$  for various values of distance  $d$ . When  $d$  is 4 Å or greater,  $c(t)$  and  $c^{(s)}(t)$  become largely invariant to further increases in  $d$ . This indicates that one can determine the thickness of the interface under different conditions by examining how the correlation function depends on distance  $d$ . Analysis of both scenarios reveals that the decay rate of the correlation function  $c^{(s)}(t)$  in Scenario 2 (IHB) surpasses that in Scenario 1 (LC).

Figure 3 displays the  $d$ -dependence of the correlation functions at three reference time points  $t^* = 1, 2, 5$  (ps). This

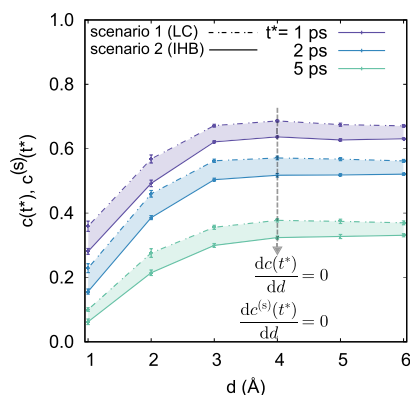


**Figure 3.** Dependence of the correlation functions on the distance  $d$  at three reference time points  $t^* = 1, 2, 5$  (ps) provides key insights into the dynamics of the air–water interface: (i) As  $d$  increases, both  $c(t^*)$  and  $c^{(s)}(t^*)$  exhibit an upward trend, with their rates of change gradually approaching 0. (ii) At each  $t^*$ ,  $c(t)$  is consistently slightly larger than  $c^{(s)}(t)$  for the same  $d$ . (iii) Air–water interface thickness  $d_f = 4$  (Å) is determined from the  $d$ -dependence of  $c(t^*)$  and  $c^{(s)}(t^*)$ , as calculated using the LC method (dot-dashed lines) and the IHB method (solid lines), respectively.

figure provides a different perspective on  $d$ -dependence: by selecting three reference time intervals on the  $t$ -axis in Figure 2, the values of the correlation functions,  $c(t)$  and  $c^{(s)}(t)$ , at these time intervals for each  $d$  were recorded. Comparing  $c(t)$  and  $c^{(s)}(t)$  in Figure 3,  $c(t)$  in Scenario 1 is always slightly larger than  $c^{(s)}(t)$  in Scenario 2 for the same  $d$ .

In Figure 3, both  $c(t^*)$  and  $c^{(s)}(t^*)$  increase as  $d$  increases, eventually reaching a point where their change rates approach

0 for sufficiently large values of  $d$ . Since  $c(t)$  and  $c^{(s)}(t)$  serve as the upper and lower bounds of the real interface correlation function  $c^r(t^*)$  respectively, it logically follows that the  $d$ -dependence of  $c^r(t^*)$  exhibits the same trend. Consequently, we arrive at the equations  $dc/dd = 0$  for  $c(t^*)$  and  $c^{(s)}(t^*)$  with respect to  $d$ . Solving for  $C = c(t^*)$  and  $C = c^{(s)}(t^*)$  yields solutions  $d_{f1}$  and  $d_{f2}$ , respectively. Here  $d_{f1}$  and  $d_{f2}$  represent the thickness of the air–water interface as determined by the LC method and the IHB method, respectively. The average value  $d_f = (d_{f1} + d_{f2})/2$  is then obtained as the thickness of the interface for a given  $t^*$ .

The correlations  $c(t^*)$  and  $c^{(s)}(t^*)$  respectively describe the relaxation characteristics of HB dynamics within the air–water interface. For both the LC and IHB methods, the values of  $c(t^*)$  and  $c^{(s)}(t^*)$  cease to change significantly when  $d$  reaches 4 (Å), i.e.,  $d_{f1} \approx d_{f2} = 4$  (Å). Thus, we determine the thickness of the air–water interface in the simulations to be  $d_f = 4$  (Å).

**3.2. HB Reaction Rate Constants.** We further examined how the reaction rate constants of H-bonds at the air–water interface vary with  $d$ . For further details regarding the HB reaction rate constants, please refer to [Section 2](#) in Supporting Information.

In Figure 4, we compare the breaking HB reaction rate constants, <sup>84,93</sup>  $k_{LC}$  and  $k_{IHB}$ , obtained by the LC and IHB

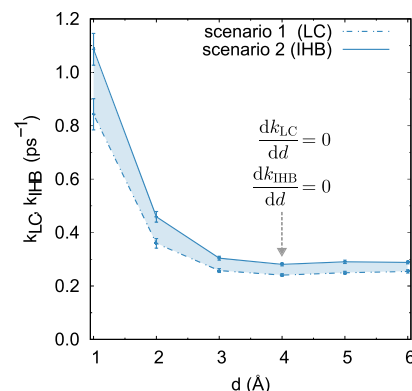


**Figure 4.** Breaking HB reaction rate constants  $k_{LC}$  and  $k_{IHB}$  for the air–water interface simulated with 512 water molecules, obtained by the LC and IHB methods, respectively. (i) Both constants,  $k_{LC}$  and  $k_{IHB}$ , decrease monotonically to the HB breaking rate  $k_{bulk}$  for the bulk water as  $d$  increases. (ii)  $k_{LC}$  is always smaller than  $k_{IHB}$  for the same  $d$ . (iii) Thickness  $d_f = 4$  (Å) of the air–water interface is obtained from the  $d$ -dependence of the rate constant  $k_{LC}$  and  $k_{IHB}$ , obtained by the LC method and the IHB method, respectively. (Consistent results for systems with 125 and 216 water molecules, please refer to the [Supporting Information](#)).

methods, respectively. We found that both constants,  $k_{LC}$  and  $k_{IHB}$ , decrease monotonically as  $d$  increases. When  $d$  is large, both rate constants  $k_{IHB}$  and  $k_{LC}$  also no longer change with  $d$ . It also shows that the HB breaking rate constant  $k_{IHB}$  is relatively larger than  $k_{LC}$ . This difference is related to the definitions of HB populations,  $h(t)$  and  $h^{(s)}(t)$ . The definition of  $h^{(s)}(t)$  leads to an increased HB break rate at the interface. The LC method retains the original rate constant of H-bonds but may include contributions from bulk water molecules.

Similar to the HB autocorrelation functions, we have the equations  $dK/dd = 0$ , for  $k_{IHB}$  and  $k_{LC}$ , with respect to  $d$ . For  $K = k_{IHB}$  and  $K = k_{LC}$ , we identify solutions  $d_{f1}'$  and  $d_{f2}'$ , respectively. Here  $d_{f1}'$  and  $d_{f2}'$  represent the HB reaction rate-based thickness of the interface obtained from the LC and IHB

method, respectively. We then calculate the thickness of the real air–water interface as  $d_f' = (d_{f1}' + d_{f2}')/2 \approx 4$  (Å). This result is supported by our calculation of the  $d$ -dependence of the HB reforming rate constants, namely,  $k_{LC}'$  and  $k_{IHB}'$ . For more details, please refer to Figure S9 in Supporting Information.

**3.3. Orientational Relaxation of the OH Stretch and Other Supports.** To verify our conclusion on the thickness of the air–water interface from the interfacial HB dynamics, we performed calculations on the orientational relaxation of the OH stretch from the perspective of anisotropy decay.<sup>96</sup>

As shown in Figure 5a, the orientation correlation function fits well with a biexponential decay function. The two

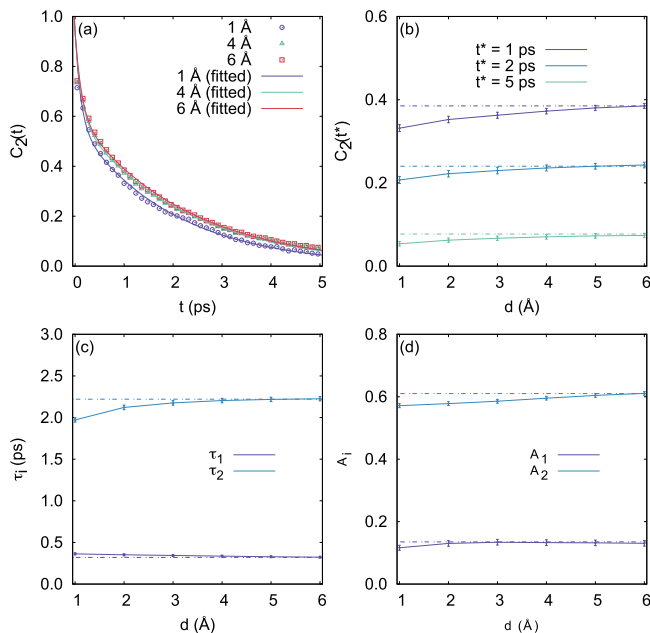


**Figure 5.** Orientation correlation function  $C_2(t)$  for the air–water interface. (a)  $C_2(t)$  for  $d = 1, 4, 6$  (Å) and the biexponential decay function  $C_2(t) = A_1 \exp(t/\tau_1) + A_2 \exp(t/\tau_2)$ .  $d$ -dependence of (b)  $C_2(t^*)$  for water molecules at the air–water interface with  $t^* = 1, 2, 5$  (ps); (c) relaxation time ( $\tau_1$  and  $\tau_2$ ), and (d) the amplitude ( $A_1$  and  $A_2$ ). Dotted line is a horizontal line for easier viewing. As  $d$  increases to  $d = 4$  (Å),  $C_2(t^*)$  and  $\tau_\nu$ ,  $A_i$  all converge to a fixed value, respectively. (We also obtained consistent results for systems with 125 and 216 water molecules, please refer to Supporting Information.).

relaxation rates ( $1/\tau_1$  and  $1/\tau_2$ ) differ; the larger relaxation time  $\tau_2$  increases with the increase of  $d$ , while the smaller one,  $\tau_1$ , remains relatively unchanged with variations in  $d$ . In Figure 5b, the values of the orientational correlation function  $C_2(t) = \langle P_2(\hat{u}(0)\hat{u}(t)) \rangle$  at three reference time  $t^* = 1, 2, 5$  (ps) are plotted. At all these times,  $C_2(t^*)$  increases with increasing  $d$  and no longer increases significantly for  $d \geq 4$  (Å).

Similar to the earlier results on HB population correlation functions and the HB reaction rates, as  $d$  increases,  $C_2(t^*)$  and associated relaxation times converge to a fixed value, respectively, which characterizes the decay time of the orientation relaxation process of OH bonds. From the convergence trend of the relaxation times and corresponding amplitudes in Figure 5c,d, we find that at the interface with a thickness greater than 4 Å, the OH orientation relaxation of the air–water interface is no longer different from bulk water.

Experimentally, the information on the interface molecules can be obtained from the SFG spectrum. The vibration relaxation time of the interface water molecules can be obtained based on the SFG spectrum using analysis techniques such as Singular Value Decomposition (SVD).<sup>97</sup> We also defined the interface molecule orientation relaxation time from the  $C_2(t)$  correlation of the interface water molecules. However, due to the arbitrariness of the specific form of defining the relaxation time, the results we obtained cannot be directly and accurately compared with the experimental results. Because of the current huge challenges in directly measuring water, we compared the data obtained from interfacial HB dynamics, interfacial OH orientation relaxation dynamics, and AIMD simulations. Our results from interfacial HB dynamics are consistent with the results from  $C_2(t)$  and density profile from AIMD simulations of the air–water interface. Furthermore, the interface thickness aligns with values obtained through experimental measurements and AIMD simulations, as detailed in Table 1. Therefore, we arrive at a consistent

**Table 1. Air–Water Interface Thickness Obtained by Experiments and Computer Simulations**

methods	T (K)	$d$ (Å)
ellipsometry (Rayleigh)	293.15	3.0
ellipsometry (Raman and Ramdas <sup>27</sup> )	293	5.0
ellipsometry (McBain et al. <sup>28</sup> )	293	$\geq 2.26$
ellipsometry (Kinoshita and Yokota <sup>29</sup> )	293	7.1
X-ray reflectivity (Braslav et al. <sup>32</sup> )	298	$3.24 \pm 0.05$
DeePMD/MB-pol/Free OH (this work)	300	5.0
BOMD/BLYP-D3/LC&IHB (this work)	300	4.0
DeePMD/MB-pol/LC&IHB (this work)	300	4.0

conclusion on the issue of estimating the thickness of the air–water interface, from the perspective of HB dynamics and OH reorientation relaxation.

There is one more aspect worth noting when studying the air–water interface based on the aforementioned definition of H-bonds. Some complications arise in interpreting vibrational SFG spectroscopy results.<sup>98</sup> An alternative perspective focusing on nonbonded OH groups better establishes a direct correlation between free OH and the  $3700\text{ cm}^{-1}$  peak, typically attributed to free OH groups.<sup>98</sup> Considering the dynamics of free OH groups, the thickness of the air–water interface is also estimated from simulations. Details on the methods and results can be found in Supporting Information. From the  $d$ -dependence of the interfacial free OH correlation function, we determined an interface thickness of approximately 5 Å. As shown in Table 1, this value slightly deviates from the main results presented in this paper, highlighting that the measured thickness of the air–water interface varies depending on the properties of interest. Thus, to accurately determine the water interface thickness, it is essential to integrate findings from these varied perspectives.

## 4. CONCLUSIONS

In this study, we have developed a two-extreme approach to investigate the HB dynamics at the air–water interface and to determine the interface's thickness. One extreme scenario underestimates the HB breaking rate constant, while the other overestimates it, implying that each scenario provides only a partial insight into the interfacial HB dynamics. Subsequently, based on DFTMD and DeePMD simulations, we have applied

our approach to two distinct system properties: HB relaxation and HB reaction rate constants at the air–water interface. Our results across both properties indicate that the predictions from both extreme scenarios converge as the thickness of the air–water interface increases to 4 Å. Thus, we have reason to believe the thickness, which falls between these two extremes, converges at this critical value.

This work introduces an approach to complement existing ones for investigating the air–water interface from a fresh perspective. Through HB dynamics of the air–water interface, interfacial properties, such as thickness in this case, can be obtained through a method analogous to the squeeze theorem. Beyond the scope of HB dynamics, this approach can be extended to other properties like molecular orientation distribution,<sup>99,100</sup> free OH dynamics,<sup>98</sup> and SFG spectrum,<sup>11,13,41</sup> or other systems like solution interfacial surfaces where statistical properties of the interface and bulk phase differ significantly. Looking ahead, this study could inspire further research into ions' hydration shells by examining ions' effects through HB dynamics.

It is important to note that our current approach focuses on probing the local environment by analyzing water pairs within HB dynamics, without considering the collective behaviors of water molecules in the HB networks. However, the collective dynamics of many water molecules have been increasingly discussed in recent research, demonstrating a close relationship with observable properties such as dielectric spectroscopy and time-dependent vibrational spectroscopy.<sup>101–106</sup> We hope our study will inspire further innovative ideas on related topics by incorporating considerations of the collective nature of water.

## ASSOCIATED CONTENT

### Data Availability Statement

The codes utilized in this study are publicly accessible on GitHub at [https://github.com/hg08/hb\\_ihb](https://github.com/hg08/hb_ihb).

### Supporting Information

The Supporting Information is available free of charge at <https://pubs.acs.org/doi/10.1021/acs.jctc.4c00457>.

Hydrogen bond correlation functions, HB breaking and reforming rate constants, details of Scenario 1: the LC method, rotational anisotropy decay of OH stretch at the air–water interface, computational methods including DFTMD and DeePMD simulations, results based on DFTMD simulations for systems in other sizes, results based on DeePMD simulations for systems in other sizes, and perspectives derived from the correlation function of free OH groups ([PDF](#))

## AUTHOR INFORMATION

### Corresponding Author

Jie Huang – Department of Applied Physics, Aalto University, Helsinki FI-00076, Finland;  [orcid.org/0000-0003-3560-283X](https://orcid.org/0000-0003-3560-283X); Email: [jie.huang@aalto.fi](mailto:jie.huang@aalto.fi)

### Author

Gang Huang – Institute of Theoretical Physics, Chinese Academy of Sciences, 100190 Beijing, China;  [orcid.org/0000-0001-8515-8584](https://orcid.org/0000-0001-8515-8584)

Complete contact information is available at:  
<https://pubs.acs.org/10.1021/acs.jctc.4c00457>

## Notes

The authors declare no competing financial interest.

## ACKNOWLEDGMENTS

This work was supported by the CSC—Chinese Government Scholarship (No. 2011113214). G.H. thanks Yuliang Jin, Rémi Khatib and Marijore Sulpizi for insightful discussions. The DFTMD simulations were conducted on the Mogon ZDV cluster in Mainz and the Cray XE6 (Hermit) at the HRLS supercomputing center in Stuttgart. The DeePMD simulations were performed on Triton, provided by Aalto Science-IT project.

## REFERENCES

- (1) Morita, A.; Hynes, J. T. A Theoretical Analysis of the Sum Frequency Generation Spectrum of the Water Surface. *J. Chem. Phys.* **2000**, *120*, 258, 371–390.
- (2) Jungwirth, P.; Tobias, D. J. Molecular Structure of Salt Solutions: A New View of the Interface with Implications for Heterogeneous Atmospheric Chemistry. *J. Phys. Chem. B* **2001**, *105*, 10468–10472.
- (3) Wilson, K. R.; Schaller, R. D.; Co, D. T.; Saykally, R. J.; Rude, B. S.; Catalano, T.; Bozek, J. D. Surface Relaxation in Liquid Water and Methanol Studied by X-Ray Absorption Spectroscopy. *J. Chem. Phys.* **2002**, *117*, 7738–7744.
- (4) Raymond, E. A.; Tarbuck, T. L.; Brown, M. G.; Richmond, G. L. Hydrogen-Bonding Interactions at the Vapor/Water Interface Investigated by Vibrational Sum-Frequency Spectroscopy of HOD/H<sub>2</sub>O/D<sub>2</sub>O Mixtures and Molecular Dynamics Simulations. *J. Phys. Chem. B* **2003**, *107*, 546–556.
- (5) Shen, Y. R.; Ostrovskikh, V. Sum-Frequency Vibrational Spectroscopy on Water Interfaces: Polar Orientation of Water Molecules at Interfaces. *Chem. Rev.* **2006**, *106*, 1140–1154.
- (6) Smits, M.; Ghosh, A.; Sterrer, M.; Müller, M.; Bonn, M. Ultrafast Vibrational Energy Transfer between Surface and Bulk Water at the Air-Water Interface. *Phys. Rev. Lett.* **2007**, *98*, No. 098302.
- (7) Sovago, M.; Campen, R. K.; Wurpel, G. W. H.; Müller, M.; Bakker, H. J.; Bonn, M. Vibrational Response of Hydrogen-Bonded Interfacial Water is Dominated by Intramolecular Coupling. *Phys. Rev. Lett.* **2008**, *100*, No. 173901.
- (8) Sovago, M.; Kramer Campen, R.; Bakker, H. J.; Bonn, M. Hydrogen Bonding Strength of Interfacial Water Determined with Surface Sum-Frequency Generation. *Chem. Phys. Lett.* **2009**, *470*, 7–12.
- (9) Stiopkin, I. V.; Weeraman, C.; Pieniazek, P. A.; Shalhout, F. Y.; Skinner, J. L.; Benderskii, A. V. Hydrogen Bonding at the Water Surface Revealed by Isotopic Dilution Spectroscopy. *Nature* **2011**, *474*, 192.
- (10) Hsieh, C.-S.; Campen, R. K.; Vila Verde, A. C.; Bolhuis, P.; Nienhuys, H.-K.; Bonn, M. Ultrafast Reorientation of Dangling OH Groups at the Air-Water Interface Using Femtosecond Vibrational Spectroscopy. *Phys. Rev. Lett.* **2011**, *107*, No. 116102.
- (11) Nihonyanagi, S.; Ishiyama, T.; Lee, T.-K.; Yamaguchi, S.; Bonn, M.; Morita, A.; Tahara, T. Unified Molecular View of the Air/Water Interface Based on Experimental and Theoretical  $\chi^{(2)}$  Spectra of an Isotopically Diluted Water Surface. *J. Am. Chem. Soc.* **2011**, *133*, 16875–16880.
- (12) Singh, P. C.; Nihonyanagi, S.; Yamaguchi, S.; Tahara, T. Interfacial Water in the Vicinity of a Positively Charged Interface Studied by Steady-State and Time-Resolved Heterodyne-Detected Vibrational Sum Frequency Generation. *J. Chem. Phys.* **2014**, *141*, 18C527.
- (13) Nihonyanagi, S.; Kusaka, R.; Inoue, K.-i.; Adhikari, A.; Yamaguchi, S.; Tahara, T. Accurate Determination of Complex  $\chi^{(2)}$  Spectrum of the Air/Water Interface. *J. Chem. Phys.* **2015**, *143*, 124707.
- (14) Ishiyama, T. Energy Relaxation Path of Excited Free OH Vibration at an Air/Water Interface Revealed by Nonequilibrium Ab

- Initio Molecular Dynamics Simulation. *J. Chem. Phys.* **2021**, *154*, 104708.
- (15) Ahmed, M.; Nihonyanagi, S.; Tahara, T. Ultrafast Vibrational Dynamics of the Free OD at the Air/Water Interface: Negligible Isotopic Dilution Effect but Large Isotope Substitution Effect. *J. Chem. Phys.* **2022**, *156*, 224701.
- (16) Omranpour, A.; Hijes, D.; Montero, P.; Behler, J.; Dellago, C. Perspective: Atomistic Simulations of Water and Aqueous Systems with Machine Learning Potentials. *arXiv* **2024**. preprint arXiv:2401.17875.
- (17) Lee, C.; McCammon, J. A.; Rossky, P. J. The Structure of Liquid Water at an Extended Hydrophobic Surface. *J. Chem. Phys.* **1984**, *80*, 4448–4455.
- (18) Dang, L. X.; Chang, T.-M. Molecular Dynamics Study of Water Clusters, Liquid, and Liquid-Vapour Interface of Water with Many-Body Potentials. *J. Chem. Phys.* **1997**, *106*, 8149.
- (19) Hsieh, C.-S.; Campen, R. K.; Okuno, M.; Backus, E. H. G.; Nagata, Y.; Bonn, M. Mechanism of Vibrational Energy Dissipation of Free OH Groups at the Air-Water Interface. *Proc. Natl. Acad. Sci. U.S.A.* **2013**, *110*, 18780–18785.
- (20) Liu, P.; Harder, E.; Berne, B. J. Hydrogen-Bond Dynamics in the Air-Water Interface. *J. Phys. Chem. B* **2005**, *109*, 2949–2955.
- (21) Gan, W.; Wu, D.; Zhang, Z.; Feng, R.-r.; Wang, H.-f. Polarization and Experimental Configuration Analyses of Sum Frequency Generation Vibrational Spectra, Structure, and Orientational Motion of the Air/Water Interface. *J. Chem. Phys.* **2006**, *124*, 114705.
- (22) McGuire, J. A.; Shen, Y. R. Ultrafast Vibrational Dynamics at Water Interfaces. *Science* **2006**, *313*, 1945–1948.
- (23) Singh, P. C.; Nihonyanagi, S.; Yamaguchi, S.; Tahara, T. Communication: Ultrafast Vibrational Dynamics of Hydrogen Bond Network Terminated at the Air/Water Interface: A Two-Dimensional Heterodyne-Detected Vibrational Sum Frequency Generation Study. *J. Chem. Phys.* **2013**, *139*, 161101.
- (24) Inoue, K.-i.; Ishiyama, T.; Nihonyanagi, S.; Yamaguchi, S.; Morita, A.; Tahara, T. Efficient Spectral Diffusion at the Air/Water Interface Revealed by Femtosecond Time-Resolved Heterodyne-Detected Vibrational Sum Frequency Generation Spectroscopy. *J. Phys. Chem. Lett.* **2016**, *7*, 1811–1815.
- (25) Jeon, J.; Hsieh, C.-S.; Nagata, Y.; Bonn, M.; Cho, M. Hydrogen Bonding and Vibrational Energy Relaxation of Interfacial Water: A Full DFT Molecular Dynamics Simulation. *J. Chem. Phys.* **2017**, *147*, No. 044707.
- (26) Ojha, D.; Kühne, T. Hydrogen Bond Dynamics of Interfacial Water Molecules Revealed from Two-Dimensional Vibrational Sum-Frequency Generation Spectroscopy. *Sci. Rep.* **2021**, *11*, 2456.
- (27) Raman, C.; Ramdas, L. On the Thickness of the Optical Transition Layer in Liquid Surfaces. *Philos. Mag.* **1927**, *3*, 220.
- (28) McBain, J. W.; Bacon, R. C.; Bruce, H. D. Optical Surface Thickness of Pure Water. *J. Chem. Phys.* **1939**, *7*, 818–823.
- (29) Kinoshita, K.; Yokota, H. Temperature Dependence of the Optical Surface Thickness of Water. *J. Phys. Soc. Jpn.* **1965**, *20*, 1086.
- (30) Fumagalli, L.; Esfandiar, A.; Fabregas, R.; Hu, S.; Ares, P.; Janardanan, A.; Yang, Q.; B, R.; Taniguchi, T.; Watanabe, K.; Gomila, G.; Novoselov, K. S.; Geim, A. K. Anomalously Low Dielectric Constant of Confined Water. *Science* **2018**, *360*, 1339–1342.
- (31) Braslav, A.; Deutsch, M.; Pershan, P. S.; Weiss, A. H.; Als-Nielsen, J.; Bohr, J. Surface Roughness of Water Measured by X-Ray Reflectivity. *Phys. Rev. Lett.* **1985**, *54*, 114–117.
- (32) Braslav, A.; Pershan, P. S.; Swislow, G.; Ocko, B. M.; Als-Nielsen, J. Capillary Waves on the Surface of Simple Liquids Measured by X-Ray Reflectivity. *Phys. Rev. A* **1988**, *38*, 2457–2470.
- (33) Superfine, R.; Huang, J. H.; Shen, Y. R. Nonlinear Optical Studies of the Pure Liquid/Vapor Interface: Vibrational Spectra and Polar Ordering. *Phys. Rev. Lett.* **1991**, *66*, 1066–1069.
- (34) Du, Q.; Superfine, R.; Freysz, E.; Shen, Y. R. Vibrational Spectroscopy of Water at the Vapor/Water Interface. *Phys. Rev. Lett.* **1993**, *70*, 2313–2316.
- (35) Ostroverkhov, V.; Waychunas, G. A.; Shen, Y. R. New Information on Water Interfacial Structure Revealed by Phase-Sensitive Surface Spectroscopy. *Phys. Rev. Lett.* **2005**, *94*, No. 046102.
- (36) Groenzin, H.; Li, I.; Buch, V.; Shultz, M. J. The Single-Crystal, Basal Face of Ice Ih Investigated with Sum Frequency Generation. *J. Chem. Phys.* **2007**, *127*, 214502.
- (37) Shen, Y. R. Basic Theory of Surface Sum-Frequency Generation. *J. Phys. Chem. C* **2012**, *116*, 15505–15509.
- (38) Ishiyama, T.; Takahashi, H.; Morita, A. Origin of Vibrational Spectroscopic Response at Ice Surface. *J. Phys. Chem. Lett.* **2012**, *3*, 3001.
- (39) Shen, Y. R. Phase-Sensitive Sum-Frequency Spectroscopy. *Annu. Rev. Phys. Chem.* **2013**, *64*, 129–150.
- (40) Ohto, T.; Usui, K.; Hasegawa, T.; Bonn, M.; Nagata, Y. Toward Ab Initio Molecular Dynamics Modeling for Sum-Frequency Generation Spectra; an Efficient Algorithm based on Surface-Specific Velocity-Velocity Correlation Function. *J. Chem. Phys.* **2015**, *143*, 124702.
- (41) Tang, F.; Ohto, T.; Sun, S.; Rouxel, J. R.; Imoto, S.; Backus, E. H. G.; Mukamel, S.; Bonn, M.; Nagata, Y. Molecular Structure and Modeling of Water-Air and Ice-Air Interfaces Monitored by Sum-Frequency Generation. *Chem. Rev.* **2020**, *120*, 3633–3667.
- (42) Kuo, I.-F. W.; Mundy, C. J.; Eggemann, B. L.; McGrath, M. J.; Siepmann, J. I.; Chen, B.; Vieceli, J.; Tobias, D. J. Structure and Dynamics of the Aqueous Liquid-Vapor Interface: A Comprehensive Particle-Based Simulation Study. *J. Phys. Chem. B* **2006**, *110*, 3738–3746.
- (43) Wick, C. D.; Kuo, I.-F. W.; Mundy, C. J.; Dang, L. X. The Effect of Polarizability for Understanding the Molecular Structure of Aqueous Interfaces. *J. Chem. Theory Comput.* **2007**, *3*, 2002–2010.
- (44) Morita, A.; Garrett, B. C. Molecular Theory of Mass Transfer Kinetics and Dynamics at Gas-Water Interface. *Fluid Dyn. Res.* **2008**, *40*, 459.
- (45) Sedlmeier, F.; Horinek, D.; Netz, R. R. Nanoroughness, Intrinsic Density Profile, and Rigidity of the Air-Water Interface. *Phys. Rev. Lett.* **2009**, *103*, No. 136102.
- (46) Fan, Y.; Chen, X.; Yang, L.; Cremer, P. S.; Gao, Y. Q. On the Structure of Water at the Aqueous/Air Interface. *J. Phys. Chem. B* **2009**, *113*, 11672–11679.
- (47) Ishiyama, T.; Morita, A. Analysis of Anisotropic Local Field in Sum Frequency Generation Spectroscopy with the Charge Response Kernel Water Model. *J. Chem. Phys.* **2009**, *131*, 244714.
- (48) Willard, A. P.; Chandler, D. Instantaneous Liquid Interfaces. *J. Phys. Chem. B* **2010**, *114*, 1954.
- (49) Vila Verde, A.; Bolhuis, P. G.; Campen, R. K. Statics and Dynamics of Free and Hydrogen-Bonded OH Groups at the Air/Water Interface. *J. Phys. Chem. B* **2012**, *16*, 9467–9481.
- (50) Ishiyama, T.; Morita, A.; Tahara, T. Molecular Dynamics Study of Two-Dimensional Sum Frequency Generation Spectra at Vapor/Water Interface. *J. Chem. Phys.* **2015**, *142*, 212407.
- (51) Nagata, Y.; Hasegawa, T.; Backus, E. H. G.; Usui, K.; Yoshimune, S.; Ohto, T.; Bonn, M. The Surface Roughness, but not the Water Molecular Orientation Varies with Temperature at the Water-Air Interface. *Phys. Chem. Chem. Phys.* **2015**, *17*, 23559.
- (52) Kühne, T. D.; Pascal, T. A.; Kaxiras, E.; Jung, Y. New Insights into the Structure of the Vapor/Water Interface from Large-Scale First-Principles Simulations. *J. Phys. Chem. Lett.* **2011**, *2*, 105–113.
- (53) Nagata, Y.; Pool, R. E.; Backus, E. H. G.; Bonn, M. Nuclear Quantum Effects Affect Bond Orientation of Water at the Water-Vapor Interface. *Phys. Rev. Lett.* **2012**, *109*, No. 226101.
- (54) Kessler, J.; Elgarbary, H.; Spura, T.; Karhan, K.; Partovi-Azar, P.; Hassanali, A. A.; Kühne, T. D. Structure and Dynamics of the Instantaneous Water/Vapor Interface Revisited by Path-Integral and Ab Initio Molecular Dynamics Simulations. *J. Phys. Chem. B* **2015**, *119*, 10079–10086.
- (55) Ohto, T.; Dodia, M.; Xu, J.; Imoto, S.; Tang, F.; Zysk, F.; Kühne, T. D.; Shigeta, Y.; Bonn, M.; Nagata, Y. Accessing the Accuracy of Density Functional Theory through Structure and

- Dynamics of the Water-Air Interface. *J. Phys. Chem. Lett.* **2019**, *10*, 4914–4919.
- (56) Jungwirth, P.; Tobias, D. J. Specific Ion Effects at the Air/Water Interface. *Chem. Rev.* **2006**, *106*, 1259–1281.
- (57) Baer, M. D.; Kuo, I.-F. W.; Tobias, D. J.; Mundy, C. J. Toward a Unified Picture of the Water Self-Ions at the Air-Water Interface: A Density Functional Theory Perspective. *J. Phys. Chem. B* **2014**, *118*, 8364–8372.
- (58) Nguyen, C. V.; Nakahara, H.; Phan, C. M. Surface Potential of the Air/Water Interface. *J. Oleo Sci.* **2020**, *69*, 519–528.
- (59) Peng, Y.; Tong, Z.; Yang, Y.; Sun, C. Q. The Common and Intrinsic Skin Electric-Double-Layer (EDL) and Its Bonding Characteristics of Nanostructures. *Appl. Surf. Sci.* **2021**, *539*, No. 148208.
- (60) Townsend, R. M.; Gryko, J.; Rice, S. A. Structure of the Liquid-Vapor Interface of Water. *J. Chem. Phys.* **1985**, *82*, 4391–4392.
- (61) Wilson, M. A.; Pohorille, A.; Pratt, L. R. Molecular Dynamics of the Water Liquid-Vapor Interface. *J. Phys. Chem.* **1987**, *91*, 4873–4878.
- (62) Matsumoto, M.; Kataoka, Y. Study on Liquid-Vapor Interface of Water. I. Simulational Results of Thermodynamic Properties and Orientational Structure. *J. Chem. Phys.* **1988**, *88*, 3233–3245.
- (63) Townsend, R. M.; Rice, S. A. Molecular Dynamics Studies of the Liquid-Vapor Interface of Water. *J. Chem. Phys.* **1991**, *94*, 2207–2218.
- (64) Lie, G. C.; Grigoras, S.; Dang, L. X.; Yang, D.; McLean, A. D. Monte Carlo Simulation of the Liquid-Vapor Interface of Water Using an Ab Initio Potential. *J. Chem. Phys.* **1993**, *99*, 3933–3937.
- (65) Alejandre, J.; Tildesley, D. J.; Chapela, G. A. Molecular Dynamics Simulation of the Orthobaric Densities and Surface Tension of Water. *J. Chem. Phys.* **1995**, *102*, 4574–4583.
- (66) Taylor, R. S.; Dang, L. X.; Garrett, B. C. Molecular Dynamics Simulations of the Liquid/Vapor Interface of SPC/E Water. *J. Phys. Chem.* **1996**, *100*, 11720–11725.
- (67) Dang, L. X.; Chang, T.-M. Molecular Dynamics Study of Water Clusters, Liquid, and Liquid-Vapor Interface of Water with Many-Body Potentials. *J. Chem. Phys.* **1997**, *106*, 8149–8159.
- (68) Car, R.; Parrinello, M. Unified Approach for Molecular Dynamics and Density Functional Theory. *Phys. Rev. Lett.* **1985**, *55*, 2471–2474.
- (69) Marx, D.; Hutter, J. Ab Initio Molecular Dynamics: Theory and Implementation. In *Modern Methods and Algorithms of Quantum Chemistry*, Grotendorst, J., Ed.; NIC Series; John von Neumann Institute for Computing: Jülich, 2000; Vol. 1, pp 301–499.
- (70) Car, R. Introduction to Density-Functional Theory and Ab-Initio Molecular Dynamics. *Quant. Struct. Act. Rel.* **2002**, *21*, 97–104.
- (71) Kuo, I.-F. W.; Mundy, C. J. An Ab Initio Molecular Dynamics Study of the Aqueous Liquid-Vapor Interface. *Science* **2004**, *303*, 658–660.
- (72) Kühne, T. D.; Krack, M.; Mohamed, F. R.; Parrinello, M. Efficient and Accurate Car-Parrinello-like Approach to Born-Oppenheimer Molecular Dynamics. *Phys. Rev. Lett.* **2007**, *98*, No. 066401.
- (73) Khalil, R. Z.; Kühne, T. D. Microscopic Properties of Liquid Water from Combined Ab Initio Molecular Dynamics and Energy Decomposition Studies. *Phys. Chem. Chem. Phys.* **2013**, *15*, 15746–15766.
- (74) Blas, F. J.; Río, E. M. D.; Miguel, E. D.; Jackson, G. An Examination of the Vapour-Liquid Interface of Associating Fluids Using a SAFT-DFT Approach. *Mol. Phys.* **2001**, *99*, 1851–1865.
- (75) Pezzotti, S.; Galimberti, D. R.; Gaigeot, M.-P. 2D H-Bond Network as the Topmost Skin to the Air-Water Interface. *J. Phys. Chem. Lett.* **2017**, *8*, 3133–3141.
- (76) Schran, C.; Thiemann, F. L.; Rowe, P.; Müller, E. A.; Marsalek, O.; Michaelides, A. Machine Learning Potentials for Complex Aqueous Systems Made Simple. *Proc. Natl. Acad. Sci. U. S. A.* **2021**, *118*, No. e2110077118.
- (77) Zeng, J.; Zhang, D.; Lu, D.; Mo, P.; Li, Z.; Chen, Y.; Rynik, M.; Huang, L.; Li, Z.; Shi, S.; Wang, Y.; Ye, H.; Tu, P.; Yang, J.; Ding, Y.; Li, Y.; Tisi, D.; Zeng, Q.; Bao, H.; Xia, Y.; Huang, J.; Muraoka, K.; Wang, Y.; Chang, J.; Yuan, F.; Bore, S. L.; Cai, C.; Lin, Y.; Wang, B.; Xu, J.; Zhu, J.-X.; Luo, C.; Zhang, Y.; Goodall, R. E. A.; Liang, W.; Singh, A. K.; Yao, S.; Zhang, J.; Wentzcovitch, R.; Han, J.; Liu, J.; Jia, W.; York, D. M.; E, W.; Car, R.; Zhang, L.; Wang, H. DeePMD-kit v2: A Software Package for Deep Potential Models. *J. Chem. Phys.* **2023**, *159*, No. 054801.
- (78) Babin, V.; Leforestier, C.; Paesani, F. Development of a "First Principles" Water Potential with Flexible Monomers: Dimer Potential Energy Surface, VRT Spectrum, and Second Virial Coefficient. *J. Chem. Theory Comput.* **2013**, *9*, 5395–5403.
- (79) Babin, V.; Medders, G. R.; Paesani, F. Development of a "First Principles" Water Potential with Flexible Monomers. II: Trimer Potential Energy Surface, Third Virial Coefficient, and Small Clusters. *J. Chem. Theory Comput.* **2014**, *10*, 1599–1607.
- (80) Medders, G. R.; Babin, V.; Paesani, F. Development of a "First-Principles" Water Potential with Flexible Monomers. III. Liquid Phase Properties. *J. Chem. Theory Comput.* **2014**, *10*, 2906–2910.
- (81) Bore, S. L.; Paesani, F. Realistic Phase Diagram of Water from "First Principles" Data-Driven Quantum Simulations. *Nat. Commun.* **2023**, *14*, 3349.
- (82) Muniz, M. C.; Gartner, I.; Thomas, E.; Riera, M.; Knight, C.; Yue, S.; Paesani, F.; Panagiotopoulos, A. Z. Vapor–Liquid Equilibrium of Water with the MB-pol Many-Body Potential. *J. Chem. Phys.* **2021**, *154*, 211103.
- (83) Medders, G. R.; Paesani, F. Dissecting the Molecular Structure of the Air/Water Interface from Quantum Simulations of the Sum-Frequency Generation Spectrum. *J. Am. Chem. Soc.* **2016**, *138*, 3912–3919.
- (84) Luzar, A.; Chandler, D. Hydrogen-Bond Kinetics in Liquid Water. *Nature* **1996**, *379*, 55–57.
- (85) Giberti, F.; Hassanali, A. A. The Excess Proton at the Air-Water Interface: The Role of Instantaneous Liquid Interfaces. *J. Chem. Phys.* **2017**, *146*, 244703.
- (86) Beaglehole, D.; Wilson, P. Thickness and Anisotropy of the Ice-Water Interface. *J. Phys. Chem.* **1993**, *97*, 11053–11055.
- (87) Sokhan, V. P.; Tildesley, D. J. The Free Surface of Water: Molecular Orientation, Surface Potential and Nonlinear Susceptibility. *Mol. Phys.* **1997**, *92*, 625–640.
- (88) Paul, S.; Chandra, A. Hydrogen Bond Dynamics at Vapour-Water and Metal-Water Interfaces. *Chem. Phys. Lett.* **2004**, *386*, 218–224.
- (89) Morita, A. Improved Computation of Sum Frequency Generation Spectrum of the Surface of Water. *J. Phys. Chem. B* **2006**, *110*, 3158–3163.
- (90) Zhao, J.; Yao, G.; Ramisetti, S. B.; Hammond, R. B.; Wen, D. Molecular Dynamics Simulation of the Salinity Effect on the n-Decane/Water/Vapor Interfacial Equilibrium. *Energy Fuels* **2018**, *32*, 11080–11092.
- (91) Serva, A.; Pezzotti, S.; Bougueroua, S.; Galimberti, D. R.; Gaigeot, M.-P. Combining Ab-Initio and Classical Molecular Dynamics Simulations to Unravel the Structure of the 2D-HB-Network at the Air-Water Interface. *J. Mol. Struct.* **2018**, *1165*, 71–78.
- (92) Madarász, A.; Rossky, P. J.; Turi, L. Excess Electron Relaxation Dynamics at Water/Air Interfaces. *J. Chem. Phys.* **2007**, *126*, 234707.
- (93) Luzar, A. Resolving the Hydrogen Bond Dynamics Conundrum. *J. Chem. Phys.* **2000**, *113*, 10663.
- (94) Benjamin, I. Hydrogen Bond Dynamics at Water/Organic Liquid Interfaces. *J. Phys. Chem. B* **2005**, *109*, 13711–13715.
- (95) Luzar, A.; Chandler, D. Structure and Hydrogen Bond Dynamics of Water–Dimethyl Sulfoxide Mixtures by Computer Simulations. *J. Chem. Phys.* **1993**, *98*, 8160–8173.
- (96) Moilanen, D. E.; Fenn, E. E.; Lin, Y.-S.; Skinner, J. L.; Bagchi, B.; Fayer, M. D. Water Inertial Reorientation: Hydrogen Bond Strength and the Angular Potential. *Proc. Natl. Acad. Sci. U.S.A.* **2008**, *105*, 5295–5300.
- (97) ichi Inoue, K.; Ahmed, M.; Nihonyanagi, S.; Tahara, T. Reorientation-Induced Relaxation of Free OH at the Air/Water

- Interface Revealed by Ultrafast Heterodyne-Detected Nonlinear Spectroscopy. *Nat. Commun.* **2020**, *11*, 5344.
- (98) Tang, F.; Ohto, T.; Hasegawa, T.; Xie, W. J.; Xu, L.; Bonn, M.; Nagata, Y. Definition of Free O–H Groups of Water at the Air–Water Interface. *J. Chem. Theory Comput.* **2018**, *14*, 357–364.
- (99) Rao, Y.; Tao, Y.-s.; Wang, H.-f. Quantitative Analysis of Orientational Order in the Molecular Monolayer by Surface Second Harmonic Generation. *J. Chem. Phys.* **2003**, *119*, 5226–5236.
- (100) Gan, W.; Wu, D.; Zhang, Z.; Feng, R.-r.; Wang, H.-f. Polarization and Experimental Configuration Analyses of Sum Frequency Generation Vibrational Spectra, Structure, and Orientational Motion of the Air/Water Interface. *J. Chem. Phys.* **2006**, *124*, 114705.
- (101) Popov, I.; Ishai, P. B.; Khamzin, A.; Feldman, Y. The Mechanism of the Dielectric Relaxation in Water. *Phys. Chem. Chem. Phys.* **2016**, *18*, 13941–13953.
- (102) Fecko, C. J.; Eaves, J. D.; Loparo, J. J.; Tokmakoff, A.; Geissler, P. L. Ultrafast Hydrogen-Bond Dynamics in the Infrared Spectroscopy of Water. *Science* **2003**, *301*, 1698–1702.
- (103) Fecko, C. J.; Loparo, J. J.; Roberts, S. T.; Tokmakoff, A. Local Hydrogen Bonding Dynamics and Collective Reorganization in Water: Ultrafast Infrared Spectroscopy of HOD/D<sub>2</sub>O. *J. Chem. Phys.* **2005**, *122*, No. 054506.
- (104) Hözl, C.; Forbert, H.; Marx, D. Dielectric Relaxation of Water: Assessing the Impact of Localized Modes, Translational Diffusion, and Collective Dynamics. *Phys. Chem. Chem. Phys.* **2021**, *23*, 20875–20882.
- (105) Offei-Danso, A.; Morzan, U. N.; Rodriguez, A.; Hassanali, A.; Jelic, A. The Collective Burst Mechanism of Angular Jumps in Liquid Water. *Nat. Commun.* **2023**, *14*, 1345.
- (106) Malosso, C.; Manko, N.; Izzo, M. G.; Baroni, S.; Hassanali, A. Evidence of Ferroelectric Features in Low-Density Supercooled Water from Ab Initio Deep Neural-Network Simulations. *Proc. Natl. Acad. Sci. U. S. A.* **2024**, *121*, No. e2407295121.



CAS BIOFINDER DISCOVERY PLATFORM™

## PRECISION DATA FOR FASTER DRUG DISCOVERY

CAS BioFinder helps you identify targets, biomarkers, and pathways

Unlock insights

**CAS**  
A division of the  
American Chemical Society